Applied Catalysis B: Environmental 231 (2018) 292–298

Contents lists available at ScienceDirect

Applied Catalysis B: Environmental

journal homepage: www.elsevier.com/locate/apcatb

Crucial support effect on the durability of $Pt/MgAl_2O_4$ for partial oxidation of methane to syngas

Fen Wang[a,b], Wei-Zhen Li[b,*], Jing-Dong Lin[a], Zhi-Qiang Chen[b], Yong Wang[a,c]

[a] National Engineering Laboratory for Green Chemical Productions of Alcohols-Ethers-Esters, Collaborative Innovation Center of Chemistry for Energy Materials, College of Chemistry and Chemical Engineering, Xiamen University, Xiamen 361005, China
[b] State Key Laboratory of Catalysis, Dalian Institute of Chemical Physics, Chinese Academy of Sciences, Dalian, 116023, China
[c] Voiland School of Chemical Engineering and Bioengineering, Washington State University, Pullman, WA 99164, United States

ARTICLE INFO

Keywords:
Platinum
$MgAl_2O_4$
Spinel
Partial oxidation of methane
Syngas
Support effect

ABSTRACT

Catalyst durability is one of the major problems hindering the commercialization of partial oxidation of methane (POM) for syngas production. We report that a $Pt/MgAl_2O_4$-HS catalyst with the $MgAl_2O_4$-HS support being synthesized via hydrolysis solvothermal (HS) method demonstrates high stability for POM during a 500 h life testing at 900 °C without detectable coke formation, while a $Pt/MgAl_2O_4$-CP counterpart in which $MgAl_2O_4$ was prepared by an optimized co-precipitation (CP) method exhibits continuous deactivation accompanied by coking. Using a suite of characterizations incluidng BET, H_2 chemisorption, XRD, STEM, TEM, TG/DTA and TPD of NH_3 and CO_2, we reveal that the high catalytic durability of the $Pt/MgAl_2O_4$-HS is due to the spinel surface of $MgAl_2O_4$-HS that can efficiently stabilize Pt against sintering. The $Pt/MgAl_2O_4$-CP, however, has defect Al_2O_3 or MgO-like species on the $MgAl_2O_4$-CP surface, inhibiting its capability to stabilize Pt. We confirm that the POM reaction undergoes a combustion-reforming pathway by monitoring the temperatures and gaseous product compositions along the catalyst bed. These results provide guidance for rational design of a longevity catalyst for POM process.

1. Introduction

Natural gas, including the fastest-growing tight gas, shale gas, and coal bed methane, rivals coal as the world's second-largest energy source [1]. Besides the direct use as clean fuel for the production of heat or electricity, natural gas can be converted to liquid fuels and chemicals via indirect syngas route. Methane is a major component of natural gas and can be converted to syngas by various technologies including partial oxidation of methane with oxygen (POM, Eq. (1)), steam reforming of methane (SRM, Eq. (2)) and dry reforming of methane with carbon dioxide (DRM, Eq. (3)), etc. POM produces syngas with a H_2/CO ratio of ~2 which is highly suitable for the synthesis of methanol or liquid fuels through a Fischer-Tropsch process [2,3]. Comprehensive analysis of the commercial SRM and other emerging processes demonstrates that POM represents the most economic technology for methanol plant even with a cryogenic air separation process [4,5].

$$CH_4 + \tfrac{1}{2}O_2 \rightarrow CO + 2H_2 \qquad \Delta H_{298K} = -36\ kJ/mol \qquad (1)$$

$$CH_4 + H_2O \rightarrow CO + 3H_2 \qquad \Delta H_{298K} = +206\ kJ/mol \qquad (2)$$

$$CH_4 + CO_2 \rightarrow 2CO + 2H_2 \qquad \Delta H_{298K} = +247\ kJ/mol \qquad (3)$$

$$CH_4 + 2O_2 \rightarrow CO_2 + 2H_2O \qquad \Delta H_{298K} = -803\ kJ/mol \qquad (4)$$

Depending on the catalyst and reaction conditions, POM seldom undergoes a direct route as showed in Eq. (1) but rather proceeds via total combustion (Eq. (4)) followed by reforming (Eq. (2), (3)) on most transition metal catalysts [2,6–9]. Since the thermal autoignition temperature of methane in excess oxygen is only 537 °C, incomplete combustion of methane in the feeding mixture (CH_4/O_2 = 2.0) with the limited oxygen is thus inevitable upon entering the high-temperature zone (> 800 °C) irrespective of accessing with the catalyst or not. In a fixed-bed reactor, the local concentrations of reactants and products change rapidly along the catalyst bed [10–12]. Oxygen is irreversibly depleted in the front part of catalyst bed and methane is subsequently consumed by steam or CO_2 reforming in the rest of the catalyst bed. The oxidation state and local structure of the transition metal catalysts also vary accordingly depending on the gaseous environment and temperature [6,13]. Taking the mostly studied Ni/Al_2O_3 catalyst as an example, $NiAl_2O_4$ and NiO/Al_2O_3 can be identified in the combustion zone while Ni/Al_2O_3 with increasing Ni particle sizes is observed in the reforming zone of the catalyst bed [14]. The formation of $NiAl_2O_4$ leads

* Corresponding author.
E-mail address: weizhenli@dicp.ac.cn (W.-Z. Li).

https://doi.org/10.1016/j.apcatb.2018.03.018
Received 26 October 2017; Received in revised form 25 December 2017; Accepted 6 March 2018
Available online 07 March 2018
0926-3373/

to deactivated combustion activity and sintering of Ni particles not only reduces catalytic activity for CO_2/H_2O reforming of methane but also facilitates carbon deposition via methane decomposition [15]. Unlike the methane steam reforming process in which carbon deposition can be efficiently suppressed by excess steam ($H_2O/CH_4 > 3$), the much dryer conditions in the POM process including SRM and DRM are not able to play the same role [7]. Among the efforts on enhancing the durability of Ni catalysts, a LiLaNiO/γ-Al_2O_3 catalyst has been developed which only exhibited a slight increase in Ni particle sizes with a small loss of Ni and Li during a 500 h life testing experiment for POM at 850 °C [16]. However, diluted reactants were used in the experiment which appears to be a major shortcoming from practical consideration. Similar to the developments on DRM catalysts, a viable strategy to reduce the Ni crystallite sizes and stabilize them against sintering under reaction conditions using undiluted reactants has yet to be established, albeit efforts have been made to modify catalysts using different precursors and pretreatments, or adding metal or oxide promoters [17–21]. Other non-noble metals and hexaaluminates and perovskites encounter similar challenges to Ni catalysts [6]. Noble metal catalysts, such as supported Pt, Pd, Rh, and Ir, are much more active at lower temperatures and more coke resistant compared to the nickel catalysts [22]. At high temperature (~1000 °C) and short contact time (10 ms), monolith-supported Rh, Pt and Ir exhibited stable activity with product selectivity far from the thermodynamic equilibrium compositions, but significant coke formation was observed over Pd [23]. Supported noble metal catalysts using $MgAl_2O_4$ as a support have shown better catalytic durability for SRM, DRM and POM [24–27], which is due to the stabilization of small noble metal nanoparticles on the $MgAl_2O_4$ spinel (111) facets [28,29]. Depending on the content of spinel (111) facets, $MgAl_2O_4$ prepared via different methods could demonstrate various efficiencies in stabilizing Pt nanoparticles [28]. Thus, a durable POM catalyst is anticipated if one can maximize the stabilization efficiency of metal nanoparticles on $MgAl_2O_4$ spinel support.

In this work, we prepared two types of Pt/$MgAl_2O_4$ catalysts by using $MgAl_2O_4$ support materials synthesized via hydrolysis solvothermal (HS) method and co-precipitation (CP) method, respectively. The catalytic activity and durability of the two catalysts for POM were evaluated at a high temperature of 900 °C with different gas hourly space velocities. The reaction mechanism on the Pt/$MgAl_2O_4$ catalyst was also studied by monitoring the axial temperature and gas compositions. The Pt/$MgAl_2O_4$-HS catalyst exhibited much higher stability in the catalyst structure and catalytic activity than the Pt/$MgAl_2O_4$-CP counterpart. We further provide insight on the intrinsic support effect on the catalyst structure and catalytic behaviour by using a suite of characterization techniques.

2. Experimental

2.1. Catalyst synthesis

$MgAl_2O_4$-HS support was prepared by hydrolysis of aluminum isopropoxide with magnesium nitrate hexahydrate in ethanol as previously reported [28]. 0.60 M of aluminum isopropoxide (≥98%, Aladdin) and 0.30 M of magnesium nitrate hexahydrate (≥99%, Damao, Tianjin, China) were mixed in 900 mL of ethanol and sealed in a 2 L autoclave. The mixture was then heated to 160 °C and held there for 5 h under vigorous stirring. After cooling to room temperature, the obtained product was filtrated and then dried at 120 °C for 2 h, and finally calcined in ambient air at 900 °C for 5 h with a heating rate of 5 °C/min. $MgAl_2O_4$-CP support was prepared by an optimized co-precipitation method with metal nitrates and ammonia. 0.07 M of magnesium nitrate hexahydrate (≥99%, Damao, Tianjin, China) and 0.14 M of aluminum nitrate nonahydrate (≥99%, Damao, Tianjin, China) were dissolved in 250 mL of deionized water under vigorous stirring to form a transparent solution. This solution and ammonia solution (25%–28%, Damao, Tianjin, China) were then simultaneously added dropwise into 100 mL of deionized water under stirring and the final pH value was adjusted to be around 10. The precipitates were aged under stirring for 24 h at room temperature. The mixture was then separated by evaporation at 90 °C instead of conventional filtration to avoid uneven loss of dissolved Mg^{2+} and Al^{3+} cations during filtration [28]. The obtained powders were further dried at 110 °C for 11 h and finally calcined at 900 °C for 5 h with a heating rate of 5 °C/min. Pt/$MgAl_2O_4$ catalysts with Pt loading of 1 wt.% were prepared by incipient wetness impregnation of 6 g of $MgAl_2O_4$-HS or $MgAl_2O_4$-CP with aqueous solution of chloroplatinic acid hexahydrate (Pt ≥ 37%, Fengchuan, Tianjin, China) at room temperature. The impregnated samples were dried at 110 °C in ambient air for 11 h, and then calcined at 500 °C for 5 h and finally reduced in H_2 at 900 °C for 2 h. Catalysts thus prepared were denoted as Pt/$MgAl_2O_4$-HS and Pt/$MgAl_2O_4$-CP, respectively. The spent catalysts after reaction at 900 °C and GHSV of 151,000 mL/(g–h) were denoted as Pt/$MgAl_2O_4$-HS-S and Pt/$MgAl_2O_4$-CP-S, respectively.

2.2. Catalyst characterization

The surface areas were measured on a Micromeritics ASAP 2460 using N_2 adsorption-desorption isotherms at −196 °C with Brunauer-Emmett-Teller (BET) method. The samples were degassed under vacuum at 350 °C for 5 h before the adsorption measurement in order to eliminate the adsorbed species. Powder X-ray diffraction (XRD) patterns of the samples were collected on a PW 3040/60 X'Pert PRO (PANalytical) diffractometer equipped with a Cu $K\alpha$ radiation source (λ = 1.5406 Å), operating at 40 kV and 40 mA. The step-scans were recorded in the 2θ range from 15° to 80° with a scanning speed of 3.84°/min. H_2 pulse chemisorption was conducted on an Auto Chem. II 2920 automatic catalyst characterization system. Prior to the chemisorption, the sample was heated with a rate of 10 °C/min to 500 °C for 2 h under 10% H_2/N_2 and then heated to 510 °C and purged with N_2 for 0.5 h before cooling down to 50 °C in N_2. The accurate Pt loadings of the catalysts were determined by inductively coupled plasma atomic emission spectroscopy (ICP-AES) on an IRIS Intrepid II XPS instrument (Thermo Electron Corporation). Scanning transmission electron microscopy (STEM) and transmission electron microscopy (TEM) analyses were performed on a JEOL JEM-2100F. TEM specimens were prepared by depositing a suspension of the powdered sample on a lacey carbon-coated copper grid. Thermogravimetric and differential thermal analyses (TG/DTA) were conducted on a TA Q600 equipment in flowing air (100 mL/min) with a heating rate of 10 °C/min. CO_2 and NH_3 temperature-programmed desorption (TPD) experiments were carried out using a Micromeritics AutoChem II 2920 Automated Catalyst Characterization System. 0.15 g of sample was placed in a quartz reactor for each test. Before introducing CO_2 or NH_3 by impulse injections, the sample was pretreated in 10% H_2/Ar flow at 500 °C for 1 h and then cooled down to 80 °C in He flow. After saturation adsorption of CO_2 or NH_3, the sample was heated in He from 80 °C to 900 °C at a heating rate of 10 °C/min and the TPD profile was recorded with a thermal conductivity detector. The areas under the TPD peaks with the normalized base line were integrated to determine the amount of desorbed CO_2 or NH_3 during TPD. The TCD response factors for NH_3 and CO_2 were obtained by analyzing the peak of given amount of the molecules, respectively.

2.3. Steady-state catalytic experiments

POM reactions were carried out at atmospheric pressure in a fixed-bed microreactor. Catalyst powders (~120 mg, 20–40 mesh) were diluted with 7.0 g of quartz sand and charged into a U-shaped quartz reactor (i.d. = 10 mm). A *k*-type thermocouple in quartz well was inserted into the catalyst bed to measure and control the temperature. Prior to reactions, the catalysts were reduced at 900 °C for 2 h in H_2 flow of 30 mL/min. After cooling the reactor to 300 °C in H_2, methane

(50 mL/min) was introduced to flush H_2 for 5 min. Then the total flow rate of the reactant gas mixture (CH_4:O_2 = 2:1) was adjusted to 74 mL/min or 302 mL/min, in order to reach a gas hourly space velocity (GHSV) of 37,000 or 151,000 mL/(g–h), respectively. The temperature was then increased to 900 °C at a ramping rate of 10 °C/min. Reactants and products were analyzed by an on-line gas chromatograph (Agilent 7890 B) equipped with a molecular sieve of 5A and a Parapak N packed column, and a thermal conductivity detector. H_2, CO, H_2O and CO_2 were detected as products in the outlet effluent. Three reaction kinetic parameters, namely CH_4 conversion (X_{CH4}), CO selectivity (S_{CO}) and the ratio of H_2 to CO (H_2/CO), were used to measure the catalytic performance. X_{CH4} was calculated from the ratio of CO and CO_2 products to total amounts of converted and unconverted CH_4 in the effluent since coke deposition is negligible on the catalysts. S_{CO} was calculated from the ratio of outlet CO concentration to the sum of CO and CO_2. H_2/CO was obtained from their molar ratio in the effluent. Carbon balance was checked by testing the Pt/$MgAl_2O_4$-CP at 900 °C and 151,000 mL/(g–h) using N_2 (2 vol%) as internal standard, which was maintained at above 97%. The difference in methane conversions calculated with and without the internal standard is less than 0.2% (Fig. S1).

2.4. Axial temperature and reaction species measurements

To measure the axial temperature and reaction species, a liftable *k*-type thermocouple in quartz well and a liftable stainless steel sampling capillary to mass spectrometer were sealed with a multiple channel connector. The liftable thermocouple and sampling capillary were initially located at the bottom of the catalyst bed and could be lifted gradually during the steady-state POM reaction. The reaction species were analyzed by an Ominstar mass spectrometer and the *m/z* of 2, 16, 18, 28, 32 and 44 were monitored to reflect the concentration of H_2, CH_4, H_2O, CO, O_2 and CO_2, respectively. The experiment was conducted at 900 °C and GHSV of 37,000 mL/(g–h) unless otherwise stated.

3. Results and discussion

3.1. Catalytic activity and stability

The catalytic performances of the Pt/$MgAl_2O_4$-HS and Pt/$MgAl_2O_4$-CP catalysts in the POM reactions were studied at a high GHSV of 151,000 mL/(g–h) and a high temperature of 900 °C. Fig. 1a displays the CH_4 conversion, CO selectivity and H_2/CO ratio as a function of time-on-stream (TOS) for these two catalysts. The Pt/$MgAl_2O_4$-CP catalyst exhibits high initial X_{CH4} (99.2%), S_{CO} (95.2%), and H_2/CO (1.94), and then gradually deactivates at about 50 h TOS with X_{CH4} and S_{CO} declining to 89% and 88%, respectively. X_{CH4} and S_{CO} suddenly drop to 83% and 85%, respectively, at the TOS of 51 h followed by continuous deactivation until 62.5 h TOS. Quick and total deactivation occurs during 62–64 h TOS and the X_{CH4} and S_{CO} reach 69% and 78%, respectively. The Pt/$MgAl_2O_4$-HS demonstrates stable catalytic performance during the entire TOS of 76 h with the X_{CH4} and S_{CO} remaining as high as 99.1-97.5% and 94.2-92.8% respectively, with the H_2/CO at about 1.89-1.86. The corresponding changes in the selectivities for CO_2, H_2 and H_2O over these two catalysts are displayed in Fig. S2. As for the catalytic activities, both Pt/$MgAl_2O_4$-HS and Pt/$MgAl_2O_4$-CP catalysts exhibit very high initial methane turnover rates of 39.5 and 54.9 mol/(mol_{Pt}-s), respectively, which were estimated by assuming the surface Pt atoms determined by H_2 chemisorption as active sites (Table 1). It should be noted that these turnover rates are not the intrinsic turnover frequencies of the catalysts since both catalysts were tested at nearly equilibrium conversions aiming at accessing the catalyst durability. A separate 500 h life study was conducted for the Pt/$MgAl_2O_4$-HS catalyst at 900 °C and a GHSV of 37,000 mL/(g–h). As shown in Fig. 1b, the X_{CH4} and S_{CO} are 99% and 96%, respectively, with H_2/CO ratio being maintained at 1.90 during the entire 500 h TOS studies, indicating that the active structures of the catalyst for POM are retained.

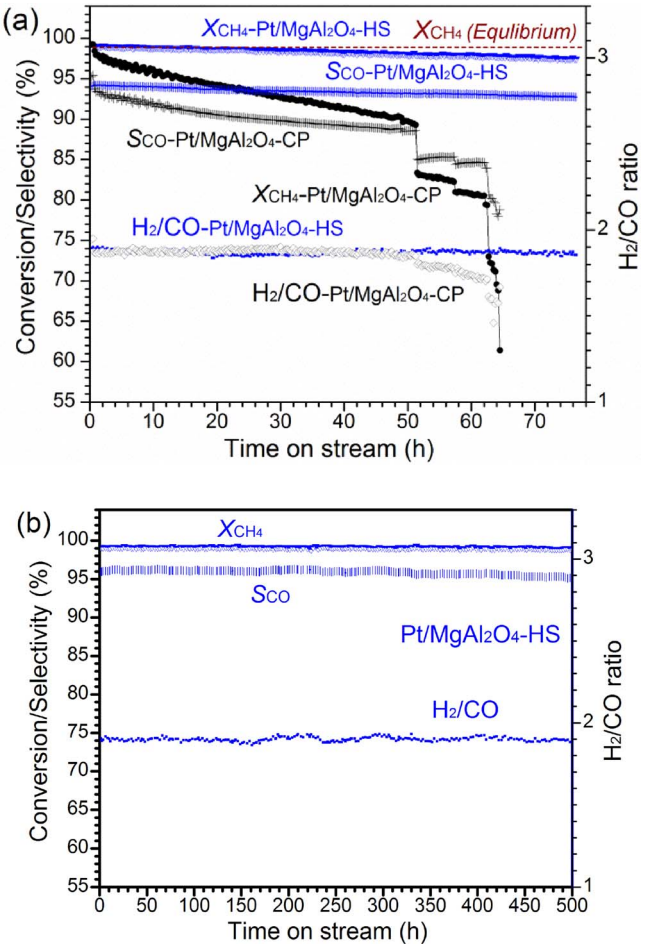

Fig. 1. (a) Catalytic performance of the Pt/$MgAl_2O_4$-HS and Pt/$MgAl_2O_4$-CP catalysts for POM as a function of time on stream at 900 °C and GHSV of 151,000 mL/(g–h); (b) Catalytic performance of the Pt/$MgAl_2O_4$-HS for POM during long-term stability test at 900 °C and GHSV of 37,000 mL/(g–h).

Table 1
Physico-chemical characteristics of the fresh and spent Pt/$MgAl_2O_4$ catalysts.

Catalyst	S_{BET} (m^2/g)	W_{Pt} (wt. %)	D_{Pt} (%)	Pt Size (nm)		d_{Spinel} (nm)
				XRD	TEM	
Pt/$MgAl_2O_4$-HS	57.5	0.96	63.7	1.9	2.3	16.9
Pt/$MgAl_2O_4$-CP	33.3	0.98	44.9	2.2	2.5	16.6
Pt/$MgAl_2O_4$-HS-S	–	–	–	12.8	2.1/11.6	22.9
Pt/$MgAl_2O_4$-CP-S	–	–	–	11.8	2.3/12.0	20.7

W_{Pt}: Pt loading; D_{Pt}: Pt dispersion; –: not test.

3.2. Axial temperature and species profiles

The reaction pathway for POM on the Pt/$MgAl_2O_4$-HS catalyst was identified by monitoring the reaction products along the catalyst bed. Fig. 2a illustrates the set-up for measuring the temperature and reaction species at different positions. The fixed thermocouple was placed in the catalyst bed at 5.5 cm below the top of catalyst bed, which was used to control the temperature at 900 °C. The MS signal intensities of the feed were collected at position "*Pa*" at room temperature. With pulling the liftable thermocouple and sampling capillary simultaneously to different positions, the temperatures and mass spectrum (MS) signals during steady-state reaction were recorded and displayed in Fig. 2b. At the position "*Pb*" which was 0.2 cm from the catalyst bed, the

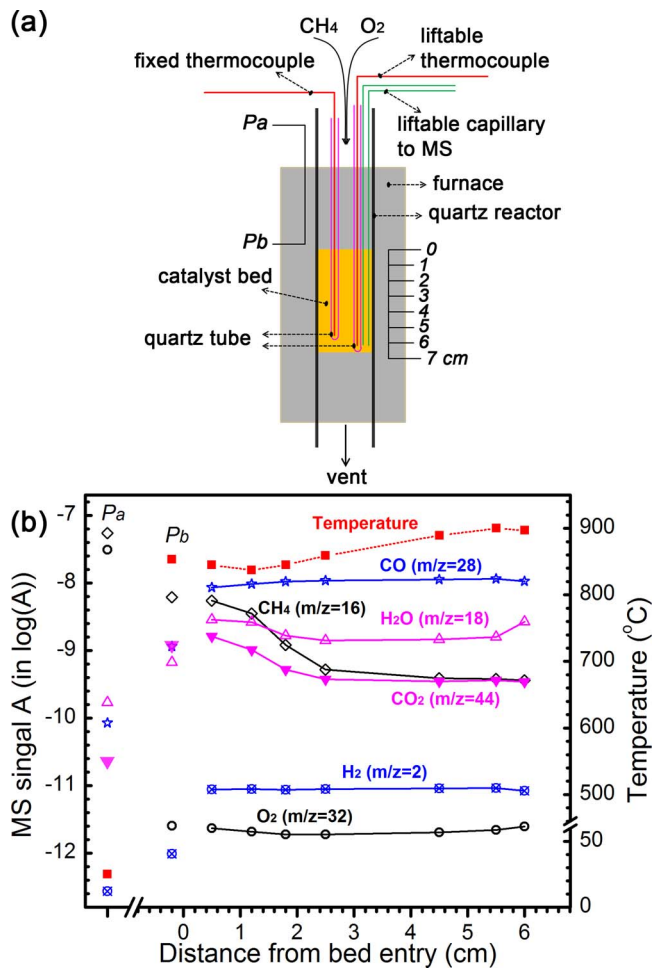

Fig. 2. (a) Schematic drawing of the reactor; (b) The axial temperature and species composition profiles in the reactor during the POM reaction on the Pt/$MgAl_2O_4$-HS catalyst at 900 °C and GHSV of 37,000 mL/(g–h).

temperature was 853 °C. The intensity of O_2 sharply decreased to a level comparable to those in the catalyst bed and the intensity of CH_4 also decreased greatly. In the meanwhile, the intensities for H_2, CO, H_2O and CO_2 increased significantly. Apparently, O_2 was totally depleted via POM (Eq. (1)) and combustion (Eq. (4)) with small fraction of methane before reaching the catalyst. With the gas stream flowing through the catalyst bed, the temperature first decreased from 853 °C at "*Pb*" to 845 °C and 837 °C, then increased to 845 °C, 859 °C, 889 °C and maximized at 900 °C when reaching the position of fixed thermocouple, and finally decreased to 897 °C at the end of the bed. The MS signal intensities of CH_4, H_2O and CO_2 decreased and those for H_2 and CO increased simultaneously along the bed. The MS signal intensity increase of CO in high concentration is more distinct in normal scale as shown in Fig. S3. The initial drop in temperature is due to endothermic SRM and DRM, leading to increased CO and H_2 concentrations accompanied by decreased H_2O and CO_2 contents. Such evolutions in the temperatures and the compositions clearly demonstrate that the reactant mixture undergoes partial oxidation and combustion of methane in the hot zone before reaching the catalyst bed and then SRM and DRM in the catalyst bed. These results are similar to the literature in which combustion of methane also occurs in the front of the catalyst bed or inert filling bed [6,30].

3.3. Catalyst characterization

The physico-chemical characteristics of the Pt/$MgAl_2O_4$ catalysts are listed in Table 1. The specific surface areas for the Pt/$MgAl_2O_4$-HS

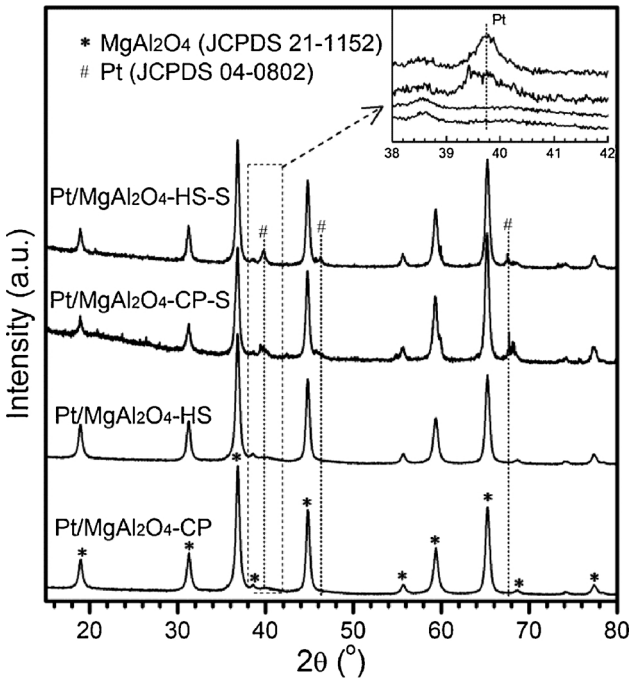

Fig. 3. XRD patterns for the fresh and spent Pt/$MgAl_2O_4$ catalysts, and the inset shows an enlarged view of the Pt (111) diffraction.

and Pt/$MgAl_2O_4$-CP are 57.5 and 33.3 m^2/g, respectively. The Pt dispersions determined by H_2 chemisorption for these two fresh catalysts are 63.7% and 44.9%, respectively. The specific surface areas and Pt dispersions for the spent catalysts were not obtained due to the limited amount of samples available. The Pt dispersions for the Pt/$MgAl_2O_4$-HS and Pt/$MgAl_2O_4$-CP after aging at 800 °C for 1 week have been reported to be 15.9% and 10.4%, respectively [28]. The average sizes of Pt particles are estimated from the broadness of their XRD peaks by using Scherrer equation. As shown in Fig. 3, very broad Pt diffractions with low intensities appear in the fresh Pt/$MgAl_2O_4$ samples while relatively sharper Pt diffractions at 39.7°, 46.3° and 67.3° are evident in the spent ones. The average sizes of Pt particles estimated by Scherrer equation using the XRD diffraction at 39.7° are 1.9 and 2.2 nm for the fresh Pt/$MgAl_2O_4$-HS and Pt/$MgAl_2O_4$-CP catalysts, respectively, while the spent Pt/$MgAl_2O_4$-HS-S and Pt/$MgAl_2O_4$-CP-S catalyst have increased Pt particle sizes of 12.8 and 11.8 nm, respectively. In addition to Pt, only crystalline $MgAl_2O_4$ spinel phase was detected in all the Pt/$MgAl_2O_4$ catalysts and the average crystalline sizes are 16–17 nm for the fresh ones and about 20–23 nm for the spent ones, displaying comparable sintering of the support during the test at 900 °C.

Fig. 4 displays the STEM images for the Pt/$MgAl_2O_4$ samples. Both the Pt/$MgAl_2O_4$-HS and Pt/$MgAl_2O_4$-CP have high Pt particle density with narrow size distributions centered at 2.3 or 2.5 nm (Fig. 4a, b), respectively. Bimodal size distributions are evident in the spent ones which are centred at 2.1 and 11.6 nm for Pt/$MgAl_2O_4$-HS-S (Fig. 4c) and at 2.3 and 12.0 nm for Pt/$MgAl_2O_4$-CP-S (Fig. 4d). These observations are highly in line with the XRD results, displaying the partial sintering of Pt particles in both catalysts. Notably, according to the relative numbers of large Pt particles to total particles shown in Fig. 4c d inset, the fractions of large Pt particles for Pt/$MgAl_2O_4$-CP-S and Pt/$MgAl_2O_4$-HS-S are 23% and 5%, respectively. This clearly indicates a less efficiency in stabilizing small Pt particles by $MgAl_2O_4$-CP compared to that of Pt/$MgAl_2O_4$-HS. Significant difference for the spent catalysts was also observed in the HRTEM images. The Pt/$MgAl_2O_4$-HS-S remained a clean rough surface (Fig. 4e) while the Pt/$MgAl_2O_4$-CP-S was covered with graphitic coke on both the surface of Pt and spinel support (Fig. 4f) [31,32].

Fig. 5 shows the TG-DTA profiles collected during heating the spent

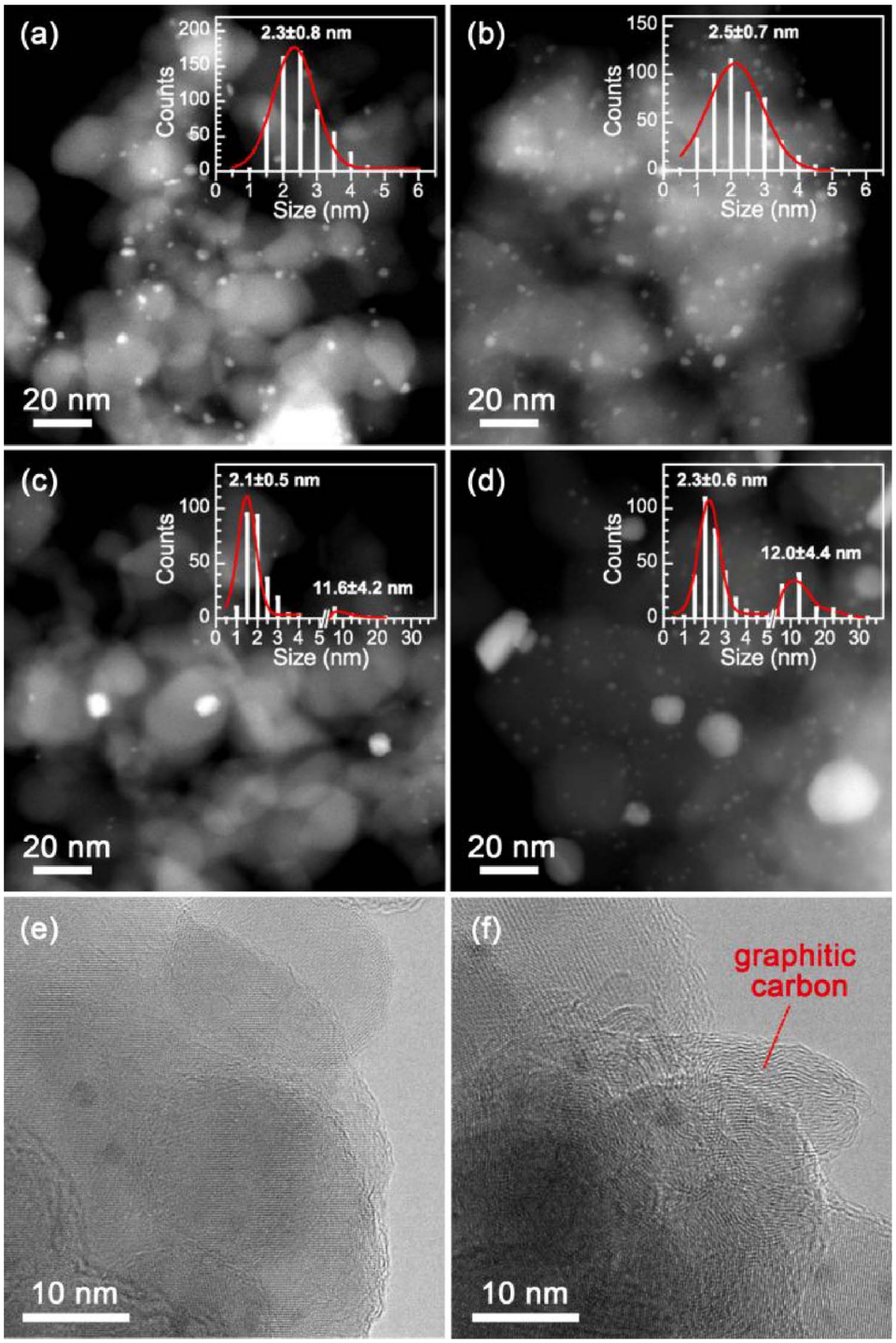

Fig. 4. STEM images for the fresh and spent catalysts. (a) $Pt/MgAl_2O_4$-HS, (b) $Pt/MgAl_2O_4$-CP, (c) $Pt/MgAl_2O_4$-HS-S and (d) $Pt/MgAl_2O_4$-CP-S, insets are Pt particle size distribution by measuring 300 particles. And TEM images of (e) $Pt/MgAl_2O_4$-HS-S and (f) $Pt/MgAl_2O_4$-CP-S.

catalysts in flowing air. $Pt/MgAl_2O_4$-HS-S catalyst shows a continuous weight loss which accumulates for about 2% without any meaningful exothermic peak, likely due to the thermal desorption of H_2O and/or CO_2 species according to the CO_2 TPD results in Fig. 6. For $Pt/MgAl_2O_4$-CP-S catalyst, in addition to the weight loss associated to desorption of H_2O and CO_2, there is a sharp weight loss of 0.9% between 600–700 °C accompanied by a distinct exothermic peak, which is due to the combustion of deposited coke. Gasification of coke occurring in this temperature range usually is the characteristic of graphitic carbon whose existence was also identified by HRTEM image as showed in Fig. 4f [33,34].

Fig. 6 shows the NH_3 and CO_2 TPD profiles for the fresh $Pt/MgAl_2O_4$ catalysts which are used to probe the difference in the surface acidity and basicity. Both catalysts present three NH_3 desorption peaks at similar temperatures but with different features. The NH_3 desorption peaks at low, medium and high temperature of 185, 360 and 600 °C were labeled as A_L, A_M and A_H, respectively. The acidic sites were calculated from the calibrated desorption peak areas which are summarized in Table 2. The acidic sites determined from A_L, A_M and A_H peaks are 2.05, 0.19 and 0.37 μmol/m^2 for the $Pt/MgAl_2O_4$-HS and 5.06, 0.15 and 0.31 μmol/m^2 for the $Pt/MgAl_2O_4$-CP, respectively. As for the CO_2 TPD profiles, the $Pt/MgAl_2O_4$-HS displays three desorption

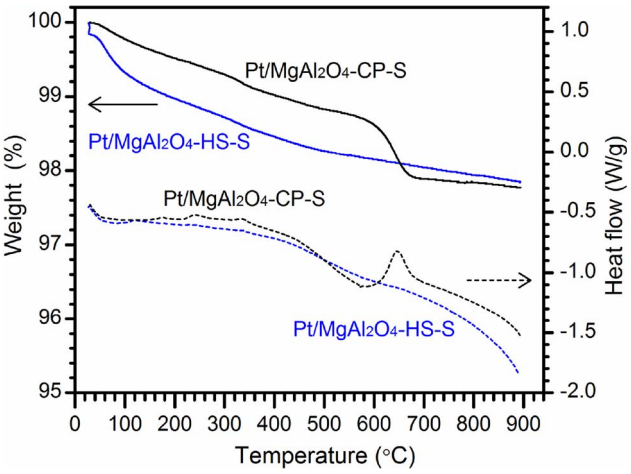

Fig. 5. TG-DTA profiles for the $Pt/MgAl_2O_4$-HS-S and $Pt/MgAl_2O_4$-CP-S catalysts.

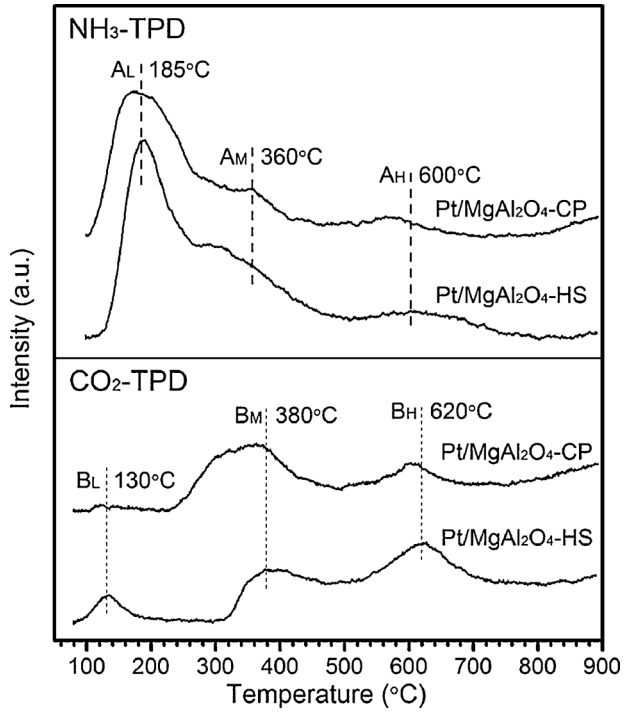

Fig. 6. NH_3 and CO_2 TPD profiles for the $Pt/MgAl_2O_4$-HS and $Pt/MgAl_2O_4$-CP catalysts.

peaks as B_L, B_M and B_H at 130, 380 and 620 °C, respectively, while the $Pt/MgAl_2O_4$-CP only provides the latter two peaks. The corresponding surface basic sites calculated from the B_L, B_M and B_H peaks are 0.05, 0.11 and 0.13 μmol/m^2 for the $Pt/MgAl_2O_4$-HS and 0, 0.48 and 0.11 μmol/m^2 for the $Pt/MgAl_2O_4$-CP, respectively. Interestingly, except the lack of CO_2 desorption at 130 °C for the $Pt/MgAl_2O_4$-CP, the onset or peak temperatures of CO_2 desorption peaks are similar to the corresponding values for NH_3 desorption peaks, indicating that the basic and acidic sites appear in pair with similar binding strength to the corresponding probe molecules. This could be caused by the coexistence of neighbouring Al and Mg cations on the various terminations of $MgAl_2O_4$ spinel crystallites which can contribute to Lewis acidic and basic sites, respectively, as the literature suggested [35]. For the Al and Mg pairs with stronger acidity and basicity, their surface ratio of Al/Mg could be roughly estimated from the A/B ratio determined by the ratio of desorbed NH_3 and CO_2. As showed in Table 2, the A_M/B_M and A_H/B_H for the $Pt/MgAl_2O_4$-HS are 1.7 and 2.8 while for the $Pt/MgAl_2O_4$-CP are 0.3 and 2.8, respectively. Notably, these values are all different from the stoichiometric ratio for Al and Mg of 2 in pure $MgAl_2O_4$, presumably because the particle surfaces are not uniform. The $MgAl_2O_4$-CP displays significant Mg rich surface in the region with medium basicity, and Al rich surface in the region with weak acidity, suggesting that the $MgAl_2O_4$-CP has much segregated Al_2O_3 or MgO domains on the surface which are not detectable by XRD and TEM. Other semiquantitative techniques such as SEM-EDS or XPS, in principle, are also not accurate enough to display the slight composition difference. Taken together, the major difference for these two samples is that the surface of $MgAl_2O_4$-HS is close to pure $MgAl_2O_4$ while the surface of $MgAl_2O_4$-CP contains Al_2O_3 or MgO impurities.

3.4. Discussion on the origin of the catalytic durability

According to the axial temperature and species analysis, the POM reaction on the $Pt/MgAl_2O_4$ catalysts undergoes a combustion-reforming pathway. The combustion is thermally ignited in the preheating zone before reaching the catalyst bed and the reforming of unreacted CH_4 by H_2O and CO_2 happens on the $Pt/MgAl_2O_4$ catalysts. Both the $Pt/MgAl_2O_4$-HS and the $Pt/MgAl_2O_4$-CP catalysts exhibit very high initial CH_4 conversion and CO selectivity with H_2/CO about 2, indicating that small Pt nanoparticles are catalytically active irrespective of the property of support material. The fact that the deactivated $Pt/MgAl_2O_4$-CP-S cannot be fully regenerated after burning the coke implies that the deactivation of the $Pt/MgAl_2O_4$-CP catalyst is most probably due to a thermal degradation of the catalyst (Fig. S4). Since coke formation at temperatures over 700 °C is mainly due to the thermal decomposition of methane [34], the coke deposition on the $Pt/MgAl_2O_4$-CP catalyst thus could be a result of the loss of catalytic reforming activity which leaves abundant unconverted CH_4 as carbon source. Compared to the $Pt/MgAl_2O_4$-CP catalyst, the $Pt/MgAl_2O_4$-HS has a much higher surface area, Pt dispersion in fresh catalyst (Table 1) and 800 °C-aged catalyst [28] is higher, and the spent catalyst after long term reaction under 900 °C has significantly smaller fraction of large Pt particles (Fig. 4 c d). Such high retainment of small Pt nanoparticles on the $Pt/MgAl_2O_4$-HS undoubtedly benefits the catalytic stability. Based on the knowledge that only $MgAl_2O_4$ spinel (111) surfaces are capable of stabilizing Pt nanoparticles against sintering at high temperatures [28], Pt particles initially not located on the (111) surfaces can readily sinter. Although the characterization results of XRD and TEM can hardly reflect the physical structure difference of these two catalysts, the NH_3 and CO_2 TPD data indeed demonstrate the intrinsic chemical difference: the $Pt/MgAl_2O_4$-CP has much more Al_2O_3 or MgO impurities on the surface than the $Pt/MgAl_2O_4$-HS. Thus, besides the lower surface area, the fraction of spinel (111) surface would be further reduced due to the possible modification with the Al_2O_3 or MgO impurities. In our previous study, a $MgAl_2O_4$-CP with XRD detectable MgO impurity has

Table 2
Acidic and basic sites calculated from the NH_3 and CO_2 TPD profiles for the $Pt/MgAl_2O_4$-HS and $Pt/MgAl_2O_4$-CP catalysts.

Catalyst	Acidic site (μmol/m^2)				Basic site (μmol/m^2)				Ratio of A/B	
	A_L	A_M	A_H	Total	B_L	B_M	B_H	Total	A_M/B_M	A_H/B_H
$Pt/MgAl_2O_4$-HS	2.05	0.19	0.37	2.61	0.05	0.11	0.13	0.30	1.7	2.8
$Pt/MgAl_2O_4$-CP	5.06	0.15	0.31	5.52	0	0.48	0.11	0.59	0.3	2.8

only retained Pt dispersion of 7.3% after aging at 800 °C for 1 week, which is significantly lower than those for the Pt/$MgAl_2O_4$-CP (10.4%) and Pt/$MgAl_2O_4$-HS (15.9%) [28]. Surface impurities on the $MgAl_2O_4$ spinel could be the major reason for the less efficiency of $MgAl_2O_4$-CP in stabilizing Pt than the $MgAl_2O_4$-HS support. As a result, continuous deactivation of the Pt/$MgAl_2O_4$-CP is not surprising. The comparison study on the support effect preliminarily explained the plausible mechanism of the deactivation of Pt catalyst supported on conventionally prepared $MgAl_2O_4$-CP with perceived "pure" spinel structure. Catalyst life can be improved by preparing $MgAl_2O_4$-HS support with surface close to spinel stoichiometry, leading to significantly improved Pt/$MgAl_2O_4$-HS catalyst.

4. Conclusions

In this work, we demonstrate a highly durable Pt/$MgAl_2O_4$-HS catalyst which exhibits excellent catalytic performance during a 500 h life test through a combustion-reforming pathway. Compared to Pt/$MgAl_2O_4$-CP counterpart which was prepared by optimized coprecipitation and has a spinel phase in bulk but with Al_2O_3 or MgO surface impurities, we report that the high durability of Pt/$MgAl_2O_4$-HS benefits from its relatively pure spinel structure both in bulk and on surface. The insights on the key elements required for stable active catalyst structure allow the design of a longevity catalyst for POM process.

Acknowledgements

This work was supported by the National Key R&D Program of China (2016YFA0202801), the National Natural Science Foundation of China (21403213, 91545114, 21376236), and the Strategic Priority Research Program of the Chinese Academy of Sciences (XDB17020100), and the "Hundred Talents Programme" of the Chinese Academy of Sciences, and the Department of Science and Technology of Liaoning province under contract of 2015020086-101. The authors thank Prof. Tao Zhang at Dalian Institute of Chemical Physics for the fruitful discussion.

Appendix A. Supplementary data

Supplementary material related to this article can be found, in the online version, at doi:https://doi.org/10.1016/j.apcatb.2018.03.018.

References

[1] Z.N. Ma, P. Ouzilleau, C. Trevisanut, C. Neagoe, S. Lotfi, D.C. Boffito, G.S. Patience, Can. J. Chem. Eng. 94 (2016) 642.
[2] A.P.E. York, T. Xiao, M.L.H. Green, Top. Catal. 22 (2003) 345.
[3] T.V. Choudhary, V.R. Choudhary, Angew. Chem. Int. Ed. 47 (2008) 1828.
[4] M.A. Pena, J.P. Gomez, J.L.G. Fierro, Appl. Catal. A Gen. 144 (1996) 7.
[5] L.M. Julian-Duran, A.P. Ortiz-Espinoza, M.M. El-Halwagi, A. Jimenez-Gutierrez, A.C.S. Sust, Chem. Eng. 2 (2014) 2338.
[6] B.C. Enger, R. Lodeng, A. Holmen, Appl. Catal. A Gen. 346 (2008) 1.
[7] S.C. Tsang, J.B. Claridge, M.L.H. Green, Catal. Today 23 (1995) 3.
[8] R.C. Jin, Y.X. Chen, W.Z. Li, W. Cui, Y.Y. Ji, C.Y. Yu, Y. Jiang, Appl. Catal. A Gen. 201 (2000) 71.
[9] R. Horn, K.A. Williams, N.J. Degenstein, A. Bitsch-Larsen, D.D. Nogare, S.A. Tupy, L.D. Schmidt, J. Catal. 249 (2007) 380.
[10] S.H. Liu, W.Z. Li, Y.Z. Wang, H.Y. Xu, Fuel Process. Technol. 89 (2008) 1345.
[11] O. Korup, C.F. Goldsmith, G. Weinberg, M. Geske, T. Kandemir, R. Schlogl, R. Horn, J. Catal. 297 (2013) 1.
[12] K. Morgan, J. Touitou, J.S. Choi, C. Coney, C. Hardacre, J.A. Pihl, C.E. Stere, M.Y. Kim, C. Stewart, A. Goguet, W.P. Partridge, ACS Catal. 6 (2016) 1356.
[13] J.D. Grunwaldt, S. Hannemann, C.G. Schroer, A. Baiker, J. Phys. Chem. B 110 (2006) 8674.
[14] D. Dissanayake, M.P. Rosynek, K.C.C. Kharas, J.H. Lunsford, J. Catal. 132 (1991) 117.
[15] H.S. Bengaard, J.K. Norskov, J. Sehested, B.S. Clausen, L.P. Nielsen, A.M. Molenbroek, J.R. Rostrup-Nielsen, J. Catal. 209 (2002) 365.
[16] S.L. Liu, G.X. Xiong, S.S. Sheng, W.S. Yang, Appl. Catal. A-Gen. 198 (2000) 261.
[17] J.M. Lavoie, Front. Chem. 2 (2014) 1.
[18] Z. Boukha, C. Jimenez-Gonzalez, M. Gil-Calvo, B. de Rivas, J.R. Gonzalez-Velasco, J.I. Gutierrez-Ortiz, R. Lopez-Fonseca, Appl. Catal. B-Environ. 199 (2016) 372.
[19] M. Gil-Calvo, C. Jimenez-Gonzalez, B. de Rivas, J.I. Gutierrez-Ortiz, R. Lopez-Fonseca, Appl. Catal. B-Environ. 209 (2017) 128.
[20] R.K. Singha, A. Shukla, A. Yadav, L.N.S. Konathala, R. Bal, Appl. Catal. B-Environ. 202 (2017) 473.
[21] A.I. Osman, J. Meudal, F. Laffir, J. Thompson, D. Rooney, Appl. Catal. B-Environ. 212 (2017) 68.
[22] M. Khajenoori, M. Rezaei, B. Nematollahi, J. Ind. Eng. Chem. 19 (2013) 981.
[23] P.M. Torniainen, X. Chu, L.D. Schmidt, J. Catal. 146 (1994) 1.
[24] D.H. Mei, V.A. Glezakou, V. Lebarbier, L. Kovarik, H.Y. Wan, K.O. Albrecht, M. Gerber, R. Rousseau, R.A. Dagle, J. Catal. 316 (2014) 11.
[25] J. Kehres, J.G. Jakobsen, J.W. Andreasen, J.B. Wagner, H.H. Liu, A. Molenbroek, J. Sehested, I. Chorkendorff, T. Vegge, J. Phys. Chem. C 116 (2012) 21407.
[26] S.C. Baek, K.W. Jun, Y.J. Lee, J.D. Kim, D.Y. Park, K.Y. Lee, Res. Chem. Intermed. 38 (2012) 1225.
[27] E.L. Foletto, R.W. Alves, S.L. Jahn, J. Power Sources 161 (2006) 531.
[28] W.Z. Li, L. Kovarik, D.H. Mei, J. Liu, Y. Wang, C.H.F. Peden, Nat. Commun. 4 (2013) 2481.
[29] W.Z. Li, L. Kovarik, D.H. Mei, M.H. Engelhard, F. Gao, J. Liu, Y. Wang, C.H.F. Peden, Chem. Mater. 26 (2014) 5475.
[30] T.H. Nguyen, A. Lamacz, A. Krzton, B. Liszka, G. Djega-Mariadassou, Appl. Catal. B-Environ. 182 (2016) 385.
[31] C.J. Liu, J.Y. Ye, J.J. Jiang, Y.X. Pan, ChemCatChem 3 (2011) 529.
[32] X.Y. Li, D. Li, H. Tian, L. Zeng, Z.J. Zhao, J.L. Gong, Appl. Catal. B-Environ. 202 (2017) 683.
[33] R.K. Singha, A. Shukla, A. Yadav, L.N.S. Konathala, R. Bal, Appl. Catal. B-Environ. 202 (2017) 473.
[34] D. Pakhare, J. Spivey, Chem. Soc. Rev. 43 (2014) 7813.
[35] L.J.I. Coleman, W. Epling, R.R. Hudgins, E. Croiset, Appl. Catal. A-Gen. 363 (2009) 52.